Science of the Total Environment 572 (2016) 98–113

Contents lists available at ScienceDirect

Science of the Total Environment

journal homepage: www.elsevier.com/locate/scitotenv

Impact of WRF model PBL schemes on air quality simulations over Catalonia, Spain

R.F. Banks *, J.M. Baldasano

[a] Earth Sciences Dept., Barcelona Supercomputing Centre - Centro Nacional de Supercomputación (BSC-CNS), Barcelona, Spain
[b] Environmental Modelling Laboratory, Technical Univ. of Catalonia, Barcelona, Spain

HIGHLIGHTS

- Planetary boundary-layer and land-surface interactions can invoke implications to air quality forecast system simulations.
- Three WRF model PBL schemes are compared to the current scheme used in the Spanish air quality forecasting system (AQFS).
- WRF PBL scheme choice show large differences in CMAQ-simulated surface pollutant concentrations.
- The Barcelona micropulse lidar (MPL), newly introduced to the NASA MPLNET, is used to validate model-simulated PBL height.
- It is found that the nonlocal ACM2 scheme may be a better choice than the current operational scheme (YSU) for complex areas.

GRAPHICAL ABSTRACT

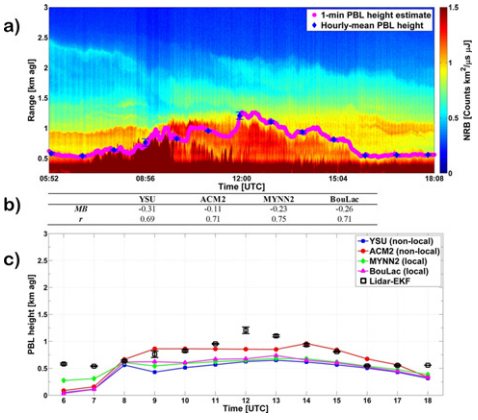

ARTICLE INFO

Article history:
Received 2 May 2016
Received in revised form 8 July 2016
Accepted 23 July 2016
Available online 3 August 2016

Editor: D. Barcelo

Keywords:
Atmospheric modelling
Weather research and forecasting (WRF) model
Remote sensing
Air quality
Lidar

ABSTRACT

Here we analyze the impact of four planetary boundary-layer (PBL) parametrization schemes from the Weather Research and Forecasting (WRF) numerical weather prediction model on simulations of meteorological variables and predicted pollutant concentrations from an air quality forecast system (AQFS). The current setup of the Spanish operational AQFS, CALIOPE, is composed of the WRF-ARW V3.5.1 meteorological model tied to the Yonsei University (YSU) PBL scheme, HERMES v2 emissions model, CMAQ V5.0.2 chemical transport model, and dust outputs from BSC-DREAM8bv2. We test the performance of the YSU scheme against the Assymetric Convective Model Version 2 (ACM2), Mellor-Yamada-Janjic (MYJ), and Bougeault-Lacarrère (BouLac) schemes. The one-day diagnostic case study is selected to represent the most frequent synoptic condition in the northeast Iberian Peninsula during spring 2015; regional recirculations. It is shown that the ACM2 PBL scheme performs well with daytime PBL height, as validated against estimates retrieved using a micro-pulse lidar system (mean bias = −0.11 km). In turn, the BouLac scheme showed WRF-simulated air and dew point temperature closer to METAR surface meteorological observations. Results are more ambiguous when simulated pollutant concentrations from CMAQ are validated against network urban, suburban, and rural background stations. The ACM2 scheme showed the lowest mean bias ($-0.96\ \mu g\ m^{-3}$) with respect to surface ozone at urban stations, while

* Corresponding author at: Earth Sciences Dept., Barcelona Supercomputing Centre - Centro Nacional de Supercomputación (BSC-CNS), Barcelona, Spain.
E-mail address: robert.banks@bsc.es (R.F. Banks).

http://dx.doi.org/10.1016/j.scitotenv.2016.07.167

the YSU scheme performed best with simulated nitrogen dioxide ($-6.48\ \mu g\ m^{-3}$). The poorest results were with simulated particulate matter, with similar results found with all schemes tested.

1. Introduction

Air quality (AQ) is of major concern worldwide for various environmental and human health effects. According to the European Environmental Agency (EEA) (Guerreiro et al., 2012) air pollutant concentrations are still too high and harm our health and the ecosystems we depend on. The EEA went on to mention that a significant proportion of Europe's population lives in areas, especially large cities, where air quality standards are routinely exceeded.

AQ forecast systems (AQFS) can be useful tools for simulating the coverage and transport of atmospheric pollutants over both global and regional unified domains. The link between emissions and ambient concentrations can only become evident and fully understood by means of air quality modelling since ground-based stations are single point. Zhang et al. (2012) reviewed the history, techniques, and state of the science of AQFS. They found that the biggest improvement in the field of AQFS is the addition of online coupling of meteorological models and chemistry models.

Numerous global and regional AQFS exist throughout Europe. Examples of global AQFS include the online LMDzt-INCA (Hauglustaine et al., 2004; Folberth et al., 2006) operated by France and ECHAM5 (Roeckner et al., 2006; Zhang et al., 2010) maintained in Germany. Regional AQFS include CHIMERE (Rouil et al., 2009) managed in France, and the CALIOPE AQFS (Baldasano et al., 2008), operated by the Barcelona Supercomputing Center (BSC-CNS) in Spain.

Boundary layer and land surface interactions have serious implications to AQFS simulations. It's well known that treatment of planetary boundary layer (PBL) processes in meteorological models have direct impacts on predicting the dynamics of pollutants (Pérez et al., 2006; Cuchiara et al., 2014). In an AQFS a few of the most important PBL variables for reliable simulations are the PBL height, wind speed and direction, temperature, and moisture. Numerical weather prediction models rely on parameterization schemes to characterize processes in the PBL.

Past works have utilized PBL parameterization schemes in the legacy fifth generation mesoscale model (MM5) to evaluate sensitivity in AQ simulations (Mao et al., 2006; Pérez et al., 2006; Bossioli et al., 2009; Kim et al., 2010). Mao et al. (2006) compared five PBL schemes from the MM5 model over the Central and Eastern United States to evaluate the sensitivity to model simulations of primary pollutant concentrations from the Community Multiscale Air Quality (CMAQ) model. Two 37-day periods were simulated in summer and winter, including a seven day spin-up period. Outputs from the CMAQ model were compared with hourly observations from 2217 AQ sites and the meteorological variables from MM5 were compared with surface and 850-hPa measurements from 50 surface sites and 21 upper-air sites. They discovered the largest sensitivity to various schemes was found with the PBL height. The Pleim-Xiu PBL scheme was on order of 800 m higher than other schemes in summer and 350 m higher in winter. This translated into AQ differences at the urban scale, with >5% differences in maximum concentration of surface ozone (O_3) and particulate matter <2.5 μm ($PM_{2.5}$).

Similar results were found by Pérez et al. (2006), where they compared three PBL schemes from the MM5 model over summertime in the Barcelona area. Meteorological outputs from the MM5 model were compared with lidar and radiosoundings measurements, while outputs from the AQFS simulations were compared with hourly observations from AQ sites, however averaged over the entire domain. They discovered that 1-h daily maximum O_3 and carbon monoxide (CO) concentrations vary in magnitude and location depending on the PBL scheme chosen. In their comparisons the O_3 bias was negative for all schemes, with a negative bias ranging from −9.1% to −14.8%. The Gayno-Seaman scheme was determined to provide the least error and lowest bias among the three compared schemes.

More recent studies have focused on the evaluation of PBL schemes in the Weather Research and Forecasting (WRF) model (Misenis and Zhang, 2010; Gan et al., 2011; Cheng et al., 2012). In Misenis and Zhang (2010) two PBL schemes; Mellor-Yamada-Janjic (MYJ) and Yonsei University (YSU), in the WRF model were compared over the Houston, Texas area for a five-day summer episode. AQ outputs were compared with hourly measurements from AQ stations and aircraft. They found 20–40% lower PBL heights with the MYJ scheme than the YSU scheme, which resulted in higher levels of CO, O_3, and $PM_{2.5}$. This was a similar finding to a study by Bossioli et al. (2009) over Athens, Greece, where PBL height predictions had 13% differences during the afternoon hours.

Another study which investigated the effects of AQ simulations to the YSU and MYJ schemes was Cheng et al. (2012). Their efforts were focused on the Taiwan area during two very different atmospheric cases in springtime; long-range transport of pollutants from a cold frontal passage and a local land-seabreeze regime. In the case of the cold frontal passage they discovered differences up to 25 ppb in O_3 concentration near the front with the simulation using the YSU scheme higher than the MYJ scheme. They attributed this difference to higher PBL heights diagnosed by the YSU scheme. In the case of local land-seabreeze effects they found that during the daytime the YSU scheme predicts a stronger seabreeze than the MYJ scheme which is more capable of carrying aged species back to land (on the order >20 ppb).

The main objective of the present study is to evaluate four PBL schemes from the WRF model and the impacts to AQ outputs in the Spanish CALIOPE AQFS. Three PBL schemes are compared to the current PBL scheme used in the operational AQFS. The paper is organized as follows. In Section 2 we describe the selected case study and the models and instruments used for the evaluation. The results of the comparison between models and observations are presented in Section 3. Finally, main conclusions are summarized in Section 4.

2. Data and methodology

2.1. Description of case study

In this study, our primary domain of interest is the area of Catalonia, Spain, located in the northeast Iberian Peninsula (IP; Fig. 1). The climate of the IP is controlled in part by thermal differences between the Atlantic Ocean to the west and the Mediterranean Sea to the east. Typical synoptic flow patterns form as a result of these differences.

The validation and comparisons presented in this work are based on data from 7 May 2015, with the time period dominated by a regional recirculations synoptic flow regime. Regional recirculations are frequent over the IP, especially in the eastern Mediterranean coast. During the spring of 2015 the phenomenon occurred approximately 33% of the days. The flow type was objectively identified using previous results (Banks et al., 2015) from a cluster analysis of back-trajectories covering a 16-yr period over Barcelona. In that particular study the authors followed the methodology of Jorba et al. (2004) for the cluster analysis algorithm. In addition, the representative day is confirmed via satellite images, lidar observations, data from air quality stations, and nearby radiosoundings. Fig. 1a shows a two-day back-trajectory analysis from

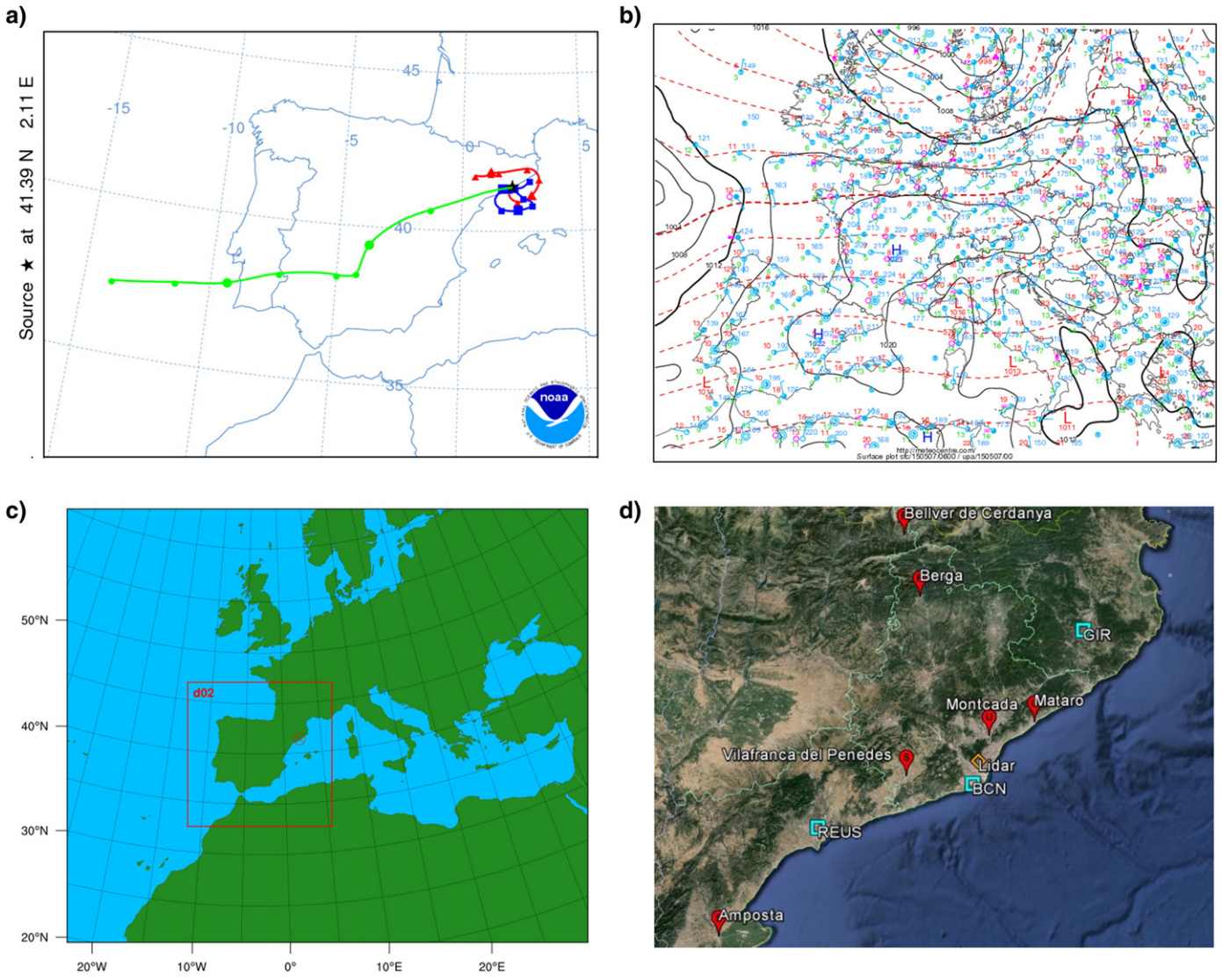

Fig. 1. a) Two-day back-trajectory analysis ending at Barcelona on 7 May 2015 (12:00 UTC) at three arriving altitudes (0.5, 1.5, and 3 km). b) Surface analysis from 6:00 UTC on 7 May 2015, including mean sea-level pressure (hPa; solid black lines), 500-hPa geopotential heights (dashed red lines), and station observations. c) two one-way nested domains for the WRF and CALIOPE AQFS at the European level (12 × 12 km), and Iberian Peninsula (4 × 4 km). d) locations of METAR (blue boxes), lidar/radiosonde (orange diamond), and air quality measurement (red circles) stations.

the NOAA Hybrid Single Particle Lagrangian Integrated Trajectory (HYSPLIT) model (Draxler and Rolph, 2013). A pattern of regional recirculations is clearly evident for back-trajectories arriving at 0.5 (red) and 1.5 (blue) km altitudes, with endpoint of Barcelona. The back-trajectory arriving at 3 km altitude (green) shows wind flow from the south-west, indicative of the main synoptic flow in the free troposphere.

Regional recirculations (Baldasano et al., 1994; Gangoiti et al., 2001) of air pollutants are typical in the summertime over the IP, but also can occur any other time during the year. Regional recirculations are generally accompanied by an absence of large-scale forcing and the pattern is dominated by mesoscale circulations, which are controlled mainly by diurnal convective heating of the atmosphere. A surface analysis of mean sea-level pressure and geopotential height at 500-hPa (Fig. 1b) at 6:00 UTC on 7 May 2015 confirms the pattern. A high pressure ridge extends south-west over north-east Spain, with light winds observed at surface stations. With this pattern the interactions between strong compensatory subsidence over the western IP and sea-land breeze dynamics are attributed to the recirculation and accumulation of pollutants.

2.2. Modelling strategy

Two domains (Fig. 1c) were configured with varying horizontal grid spacing for the CMAQ and WRF modules of the AQFS, which include the parent European level (12 × 12 km; 481 × 401 grid points), and an one-way nested domain for the IP (4 × 4 km; 399 × 399 grid points). It is assumed that 4 × 4 km grid spacing is of fine enough detail to resolve most mesoscale features in the complex study area (Pay et al., 2014; Schaap et al., 2015). Pay et al. (2014) found the forecast skill between 4 km and 1 km grid spacing was not a large improvement.

2.2.1. CALIOPE air quality forecast system

The CALIOPE AQFS (Baldasano et al., 2008; www.bsc.es/caliope), is a state-of-the-art, high-resolution operational AQFS developed in the Earth Sciences Dept. at the Barcelona Supercomputing Center - Centro Nacional de Supercomputación (BSC-CNS). The original concept of CALIOPE AQFS for the Iberian Peninsula domain (4 km × 4 km grid spacing) was funded by the Spanish Ministry of the Environment to establish an AQ forecasting system to increase the knowledge on transport and dynamics of pollutants in Spain. Since 2008, the AQ group at

BSC-CNS has added and evaluated domains for Europe (12 km × 12 km grid spacing), and for multiple regional domains (1 km × 1 km grid spacing). The system provides operational forecasts out to 24-h and 48-h depending on the domain, with a temporal resolution of 1-h.

The system has been evaluated in several past studies for the European domain (Pay et al., 2010, 2012a; Basart et al., 2012), the Spanish domain (Baldasano et al., 2008, 2011; Pay et al., 2011, 2012b, 2014; Sicardi et al., 2012), and the Barcelona and Madrid domains (Goncalves et al., 2009; Soret et al., 2011). However, the CALIOPE AQFS hasn't been evaluated for sensitivities to the various PBL schemes available in the WRF meteorological model.

The CALIOPE AQFS is constructed of four main model components. The components consist of a meteorological model (WRF-ARW v3.5.1), an emissions inventory model (HERMES v2), a chemical transport model (CMAQ v5.0.2), and a second generation mineral dust transport model (BSC-DREAM8b v2). Aerosols are estimated from CMAQ and BSC-DREAM8b. More information about the individual components of the CALIOPE AQFS can be found online (www.bsc.es/caliope).

For the evaluation we use hourly model outputs of surface ozone (O_3), nitrogen dioxide (NO_2), and particulate matter <10 μm (PM_{10}) from the CALIOPE-CMAQ simulations.

2.2.2. WRF model configuration

In this study we use WRF version 3.5.1 with the Advanced Research WRF (ARW) dynamical solver (Skamarock et al., 2005). WRF v3.5.1 is the current version used in the operational CALIOPE AQFS. Initial and lateral boundary conditions are determined using gridded Global Forecasting System (GFS) analysis data from the National Centers for Environmental Prediction (NCEP), which are operational global analysis data available on 0.25° × 0.25° grids at six-hourly time steps. The analyses are available from the surface and at 26 mandatory pressure levels from 1000 hPa to 10 hPa.

WRF-ARW simulations were computed with a 36-h forecast cycle, including 12 h allotted for model spin-up time. Each day's simulation was initialized from 12:00 UTC the previous day. The spin-up cycle is added to counter instability issues within the simulation and the first 12-h of each forecast cycle are not included in the evaluation process. An output temporal resolution of 1-h was chosen for comparison with observations. The model was run with 38 terrain-following (ETA) vertical levels, of which 13 are located in the lowest 3 km of the atmosphere, with a model top set at 50-hPa.

The HERMES emission model requires 48-h of previous meteorological fields from the date of interest. For our diagnostic case we have run the WRF model for 5–7 May 2015.

The physics options selected include WRF single-moment 3-class microphysics (Hong et al., 2004), Kain-Fritsch cumulus parametrization (Kain, 2004), Dudhia shortwave radiation (Dudhia, 1989), rapid radiative transfer model longwave radiation (Mlawer et al., 1997), and the Noah land-surface model (Tewari et al., 2004). An urban parameterization was tested, with similar results to those without an urban parameterization. More information about these physics options can be found in (Skamarock and Klemp, 2008).

In version 3.5.1 of WRF-ARW there is the option to choose from 11 PBL schemes. Each PBL scheme is associated with one or more surface-layer schemes which provide the surface fluxes of momentum, moisture, and heat to the PBL scheme. An overview of the four PBL schemes selected for this study is shown in Table 1.

The Yonsei University (YSU) PBL scheme is used in the current version of the operational CALIOPE AQFS, and will be used as the control run. The other three schemes selected showed good performance in a previous performance evaluation (Banks et al., 2015) over Barcelona. Also shown in the table are the associated surface-layer schemes, another important source of error in WRF model simulations. All four PBL schemes are associated with some variation of Monin-Obukhov similarity theory for the surface layer. Other surface layer schemes are not evaluated here.

The PBL parametrization schemes selected consist of two local and two non-local closure schemes. The operational definition of PBL height in the individual schemes falls into one of two general classes. The first class calculates the PBL height using the Richardson bulk number (Ri_b) method from some predetermined starting level. The second class determine the PBL height at a level where the turbulent kinetic energy (TKE) profile decreases to some predefined threshold value.

The first and most widely-used PBL scheme is the YSU scheme (Hong et al., 2006). The YSU scheme is a first order, non-local scheme with an explicit entrainment layer and a parabolic K-profile in an unstable mixed layer. It's a modified version of the Medium Range Forecast (MRF) scheme (Hong and Pan, 1996) from the MM5 model (Dudhia, 1993). The largest improvement to the YSU scheme over the MRF scheme was the addition of an explicit term for the treatment of the entrainment zone. (Hong, 2010) implemented a modification to the scheme for the stable boundary layer. PBL height in the YSU scheme is determined from the Ri_b method, but calculated starting from the surface. A threshold value of zero is used for stable cases, while 0.25 is used for unstable flow.

The second scheme is the Asymmetrical Convective Model version 2 (ACM2) scheme (Pleim, 2007). The ACM2 scheme is a first order, non-local closure scheme and features non-local upward mixing and local downward mixing. It's a modified version of the ACM1 scheme from the MM5 model, which was a derivative of the Blackadar scheme (Blackadar, 1978). The scheme has an eddy-diffusion component in addition to the explicit non-local transport of ACM1. PBL height is determined as the height where the Ri_b calculated above the level of neutral buoyancy exceeds a critical value ($Ri_{bc} = 0.25$). For stable or neutral flows the scheme shuts off non-local transport and uses local closure.

The third scheme is the Mellor-Yamada-Nakanishi-Niino Level 2.5 (MYNN2) scheme (Nakanishi and Niino, 2006). The Mellor-Yamada-Nakanishi-Niino Level 3 (MYNN3) scheme shares similar characteristics to MYNN2 so it will not be evaluated here. The MYNN2 scheme is tuned to a database of large eddy simulations (LES) in order to overcome the typical biases associated with other MY-type schemes, such as insufficient growth of convective boundary layer and under-estimated TKE. The MYNN2 scheme is a one-and-a-half order, local closure scheme and predicts sub-grid TKE terms. PBL height is determined as the height at which the TKE falls below a critical value (1.0×10^{-6} m^2 s^{-2}).

The fourth scheme is the Bougeault-Lacarrère (BouLac) scheme (Bougeault and Lacarrere, 1989). The BouLac scheme is a one-and-a-half order, local closure scheme and has a TKE prediction option designed for use with the BEP (Building Environment Parametrization) multi-layer, urban canopy model (Martilli et al., 2002). BouLac

Table 1
Four WRF PBL schemes evaluated in this study, including long name, turbulent kinetic energy closure type, associated surface layer scheme, and operational method and threshold value for diagnosing PBL height.

	YSU	ACM2	MYNN2	BouLac
Long name	Yonsei University	Asymmetric Convective Model v2	Mellor-Yamada-Nakanishi-Niino level 2.5	Bougeault-Lacarrère
Closure	1.0 non-local	1.0 non-local	1.5 local	1.5 local
Surface layer	Monin-Obukhov	Monin-Obukhov	MYNN	Monin-Obukhov
PBL height method	Ri_b calculated from surface	Ri_b calculated above neutral buoyancy level	TKE-prescribed threshold	TKE-prescribed threshold
Threshold	Zero (unstable) 0.25 (stable)	0.25 (all)	1.0×10^{-6} m^2 s^{-2}	5.0×10^{-3} m^2 s^{-2}

diagnoses PBL height as the height where the prognostic TKE reaches a sufficiently small value (in the current version of WRF is 0.005 $m^2 s^{-2}$).

2.3. Evaluation data

In order to validate the simulations we use data from air quality and meteorological stations, micropulse lidar, and radiosoundings. The locations of the stations are shown in Fig. 1d.

2.3.1. Air quality stations

Previous works (Pay et al., 2014; Schaap et al., 2015) have found that 4 km grid spacing is sufficient resolution for the comparison to observations. We selected a mix of six background air quality stations; evenly distributed among urban, suburban, and rural categories (red circles, Fig. 1d) for the evaluation of CALIOPE AQFS simulations. Variables compared are hourly surface concentrations of O_3, NO_2, and PM_{10}. The evaluation is taken from a statistical perspective, comparing model output to observations, and from a two-dimensional view, evaluating the spatial differences between the YSU scheme (control run) and the three other PBL schemes.

2.3.2. PBL height retrievals from lidar

Estimates of the hourly PBL height between 6:00 and 18:00 UTC are determined based on observations from a micropulse lidar (MPL) in Barcelona (orange diamond, Fig. 1d). Nighttime and early morning PBL height is not considered due to instrumental limitations (overlap range, etc.). The MPL in Barcelona is a new station in the NASA Micropulse Lidar Network (MPLNET) (Welton et al., 2001). The MPL instrument (Spinhirne et al., 1995) is operated continuously at 532-nm wavelength, using the same telescope construction to transmit an energy pulse and receive the returned backscattered signal. We exploit the lidar data at 15-m range and 1-min temporal resolutions.

The PBL height is estimated from the lidar normalized relative backscatter (NRB) using a time-adaptive extended Kalman filter technique (EKF). The EKF technique was developed and tested by the Remote Sensing Laboratory at the Technical University of Catalonia (Rocadenbosch et al., 1998, 1999). The EKF method has been evaluated by numerous studies, both with experimental and real datasets. Lange et al. (2014, 2015) tested the technique with experimental lidar simulations and real data over Barcelona. More recently the performance of the EKF method has been evaluated with observational data from Raman lidars at Barcelona (Banks et al., 2014, 2015) and Athens (Banks et al., 2016).

2.3.3. Surface and upper-air meteorology

Surface meteorological observations are collected from three area METAR stations (light blue squares, Fig. 1d) at Barcelona (41.29°N 2.07°E), Girona (41.91°N 2.76°E), and Reus (41.15°N 1.18°E). We use

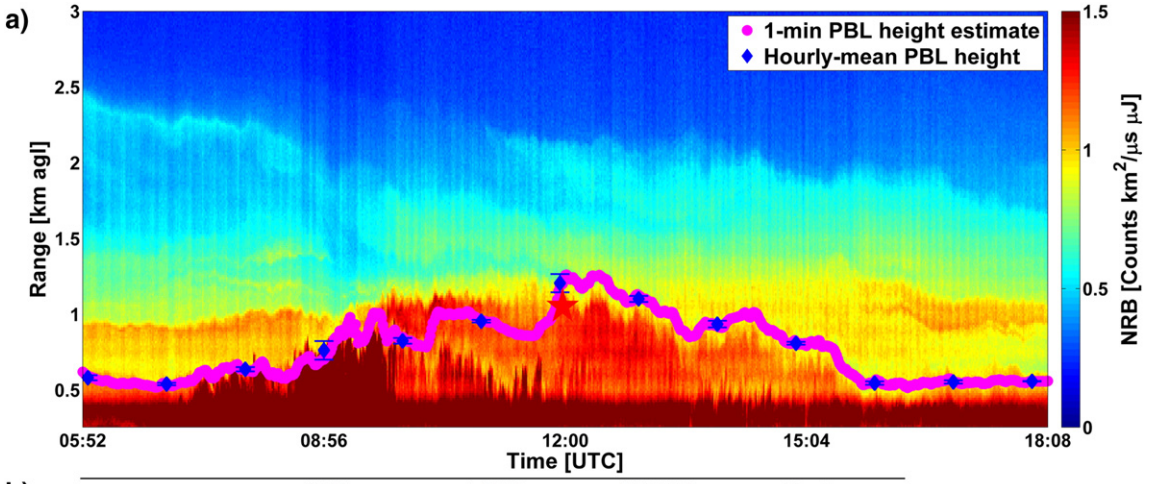

b)

	YSU	ACM2	MYNN2	BouLac
MB	-0.31	-0.11	-0.23	-0.26
r	0.69	0.71	0.75	0.71

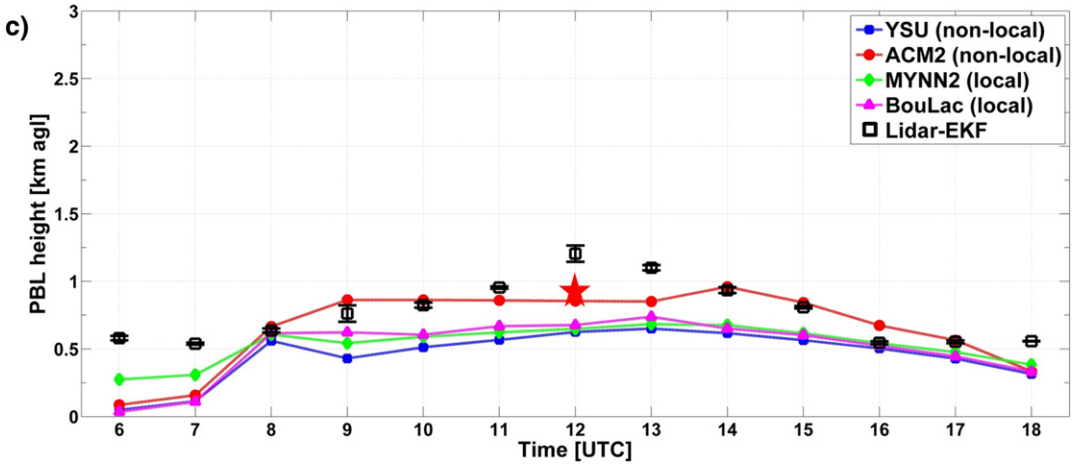

Fig. 2. a) Time-range series of lidar normalized relative backscatter (NRB), overlaid with 1-min (magenta dots) and 15-min average (blue diamonds) PBL heights. b) mean bias (*MB*; WRF – lidar) and linear correlation coefficient (*r*) between PBL heights simulated from the WRF model and estimates from the lidar. c) time series on 7 May 2015 of daytime PBL heights simulated by the WRF model and 15-min averages (black squares) from the lidar, with 1-σ error bars. PBL height estimated (bulk Richardson method) from the 12 UTC radiosonde launch is shown by the red star.

hourly measurements of 2-m air temperature (T2) and dew point temperature (TD2), along with 10-m zonal (U10) and meridional (V10) wind components to validate simulated values from the WRF model using the four PBL schemes.

For the comparisons of WRF model vertical profiles we use upper-air data from a 12:00 UTC radiosonde launch on 7 May 2015 in Barcelona, nearby to the MPL site. Upper-air variables evaluated include temperature, dew point temperature, and zonal and meridional wind components.

The collocated WRF model data are determined by finding the nearest model grid indices to each station location in longitude and latitude.

3. Results and discussion

In this section we present the results of the comparison for CALIOPE-CMAQ and WRF simulations on 7 May 2015. First, we investigate the WRF-simulated surface variables using the different WRF PBL schemes. Next, vertical profiles from WRF are compared with observations from the nearby radiosonde launch. In the last section we evaluate the photochemical and aerosol outputs from the CMAQ simulations.

3.1. Evaluation of WRF meteorology

Meteorological simulations from WRF are an important driver for air quality simulations from the CALIOPE AQFS. We evaluate the simulated PBL height from WRF, along with surface meteorological and upper-air variables.

3.1.1. PBL height

Typically, one of the largest sources of error in mesoscale model simulations is diagnosis of the PBL height. Fig. 2a shows 1-min and hourly-averaged PBL heights estimated from the MPL using the EKF technique. The mean PBL height for the day is 0.77 km with a small (0.02 km) standard deviation. Additional aerosol layers are evident between the PBL top and 2.5 km, most likely due to the regional recirculation pattern. Based upon the relatively low standard deviation we subject 15-min mean lidar-EKF estimates centered on the synoptic hour to validate PBL heights from the WRF model.

Fig. 2b,c compare the PBL heights simulated with the WRF model against hourly-averaged estimates from the MPL. It is shown the WRF model systematically under-estimates PBL height, as large as 0.31 km with the YSU scheme. The YSU and MYNN2 schemes diagnosis daytime-maximum PBL heights nearly 50% lower than the lidar. Overall, the ACM2 scheme leads to the lowest absolute bias ($MB = -0.11$ km) and closest daytime-maximum PBL height (0.96 km) compared to the lidar estimate (1.2 km). It should also be noted the WRF model simulates slow growth of the PBL, with the maximum PBL height delayed around 1–2 h compared with the lidar.

Spatial differences of PBL height between the WRF PBL schemes are also evident at 12:00 UTC on 7 May 2015 (Fig. 3). PBL height simulated using the ACM2 scheme is around 0.3 km higher than the other three schemes to the west of Barcelona and just south of Lleida. In addition, the ACM2 scheme is higher along the pre-coastal and Pyrenees mountain ranges. These results are consistent with those presented with the time series in Fig. 2c.

3.1.2. Surface meteorological variables

The 2-m air temperature (T2) and dew point temperature (TD2), and 10-m zonal (U10) and meridional (V10) wind components are also critical variables to simulate accurately to produce accurate air quality model simulations. Table 2 presents the mean bias (*MB*) and correlation coefficient (*r*) between WRF model-simulated surface meteorology and observations at the three METAR stations in Catalonia. T2 and TD2 are under-estimated by the WRF model with all PBL schemes at Barcelona and Reus, with the best performance from the BouLac scheme ($MB_{T2} = -1.68$ °C at Barcelona; $MB_{T2} = -2.34$ °C at Reus). A small over-estimate of T2 is simulated by the WRF model at Girona, as low as 0.11 °C with the MYNN2 scheme. The correlation between model and observations is markedly better with T2 ($r = 0.93$–0.98) than TD2 ($r = 0.11$–0.79).

The diurnal cycle of WRF model-simulated T2 and TD2 against observations from the three METAR stations is shown in Fig. 4. It is concluded the daily-mean over-estimate of WRF model-simulated T2 at Girona is in large part due to a significant over-estimate in the morning hours, as high as 2.68 °C at 7:00 UTC with the ACM2 scheme. The MYNN2 scheme provides the lowest bias throughout these morning hours. At Barcelona and Reus, the WRF model under-estimates T2 throughout the diurnal cycle, showing the largest biases in the morning and late evening hours.

The results are more ambiguous with respect to mean bias and correlation between WRF model-simulated U10 and V10 against observations (Table 2). The correlation between model and observations is markedly different with U10 ($r = 0.1$–0.75) versus V10 ($r = 0.87$–0.98), indicating the WRF model can resolve the meridional component of 10 m winds more reliably. The WRF model under-estimates U10 and V10 at Barcelona and Reus, no matter what PBL scheme is selected. However, the ACM2 scheme provides WRF model-simulated values closest to the observations, especially with V10 ($MB = -0.64$ m s^{-1} at Barcelona; $MB = -0.22$ m s^{-1} at Reus. Both U10 and V10 are over-estimated at Girona, with the best performance from the WRF model with the YSU scheme ($MB_{U10} = 0.43$ m s^{-1} and $MB_{V10} = 0.39$ m s^{-1}).

Finally, Fig. 5 shows the diurnal cycle of U10 and V10 simulated by the WRF model against observations from the three METAR stations.

The daily-mean over-estimate of WRF model-simulated winds at Girona is most attributable to the large deviation from the observations in the evening after 14:00 UTC, highest with model-simulated V10 with the BouLac scheme ($MB = 4.52$ m s^{-1} at 18:00 UTC).

3.1.3. Comparison of vertical profiles

We evaluate the model performance for the lower atmospheric column (up to 3 km altitude), comparing WRF model simulations to observations from a 12:00 UTC radiosonde launch (Fig. 6) for a) temperature, b) dew point temperature, and c) zonal and e) meridional winds. The WRF model systematically performs well with temperature and dew point temperature, while the largest bias between the WRF model and observations is shown with the winds.

WRF model-simulated temperature is under-estimated throughout the entire PBL, with the MYNN2 scheme showing the closest simulated values to the observations. Dew point temperature is under-estimated by the WRF model from the surface up to 1.75 km altitude, then the radiosonde observations indicate a dry layer between 2 and 2.5 km which the WRF model cannot resolve with any PBL scheme. Overall, WRF model-simulated dew point temperature with the BouLac PBL scheme has the lowest bias when compared to the observations.

The zonal wind simulated by the WRF model is under-estimated with all PBL schemes, by as much as 4 m s^{-1} with local PBL schemes. Meanwhile, the meridional wind component is under-estimated by the WRF model in the boundary layer, but over-estimated above the PBL. Large differences are shown between the various PBL schemes in the PBL, with the lowest bias from the BouLac scheme.

3.2. Air quality evaluation

First, we evaluate the spatial differences of surface O_3 concentration (Fig. 7) between the YSU scheme (control run) and the bias error (WRF scheme – control) from the three other PBL schemes at three static times during the day. The times are selected to represent the morning (6:00 UTC), afternoon (12:00 UTC), and evening (18:00 UTC) hours.

In the morning, the highest O_3 concentrations are located in the Pyrenees range near Berga and to the west. Concentrations range from 90 to 100 μg m^{-3}. Effects of the topography can be shown in the bias

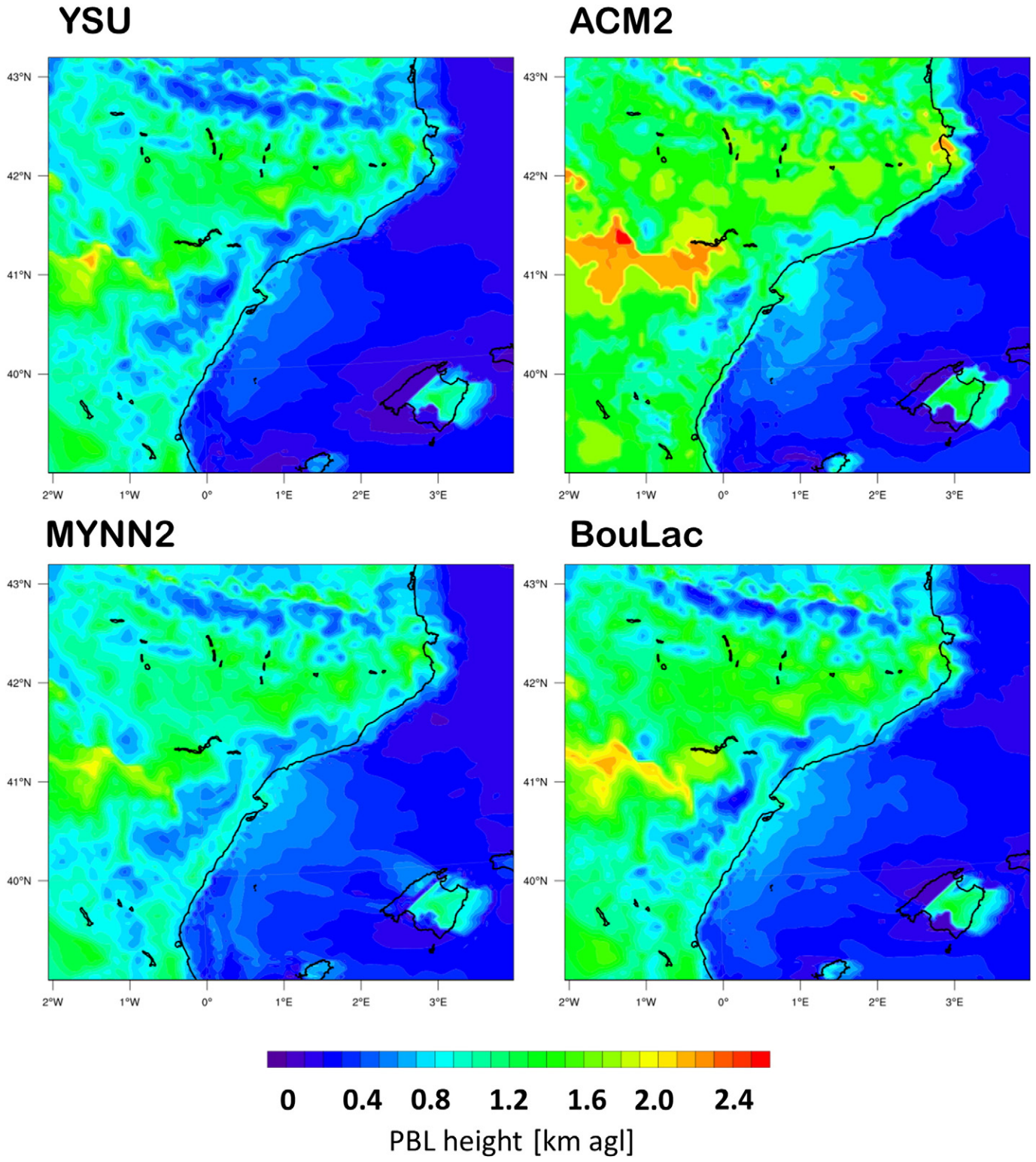

Fig. 3. PBL height (km agl) at 12:00 UTC on 7 May 2015 simulated with the WRF model using each of the four PBL schemes.

plots, most evident with the BouLac scheme. CMAQ model-simulated O_3 with the ACM2 scheme best represents the concentrations at 6:00 UTC, with a bias error <5 μg m^{-3}. At 12:00 UTC, maximum O_3 concentrations form just north-east of Barcelona (>110 μg m^{-3}) and west of Mallorca (>95 μg m^{-3}). CMAQ model-simulated O_3 with the three other PBL schemes show mainly a negative bias error (≈ -10 to -14 μg m^{-3}) near Barcelona, with a slightly smaller bias with the BouLac scheme. In addition, the CMAQ model shows a negative bias error (≈ -10 to -14 μg m^{-3}) with the plume west of Mallorca. CMAQ model simulations with the ACM2, MYNN2, and BouLac schemes all show similar bias errors. Three areas of maximum surface O_3 concentrations have formed by the evening (18:00 UTC); over the Pyrenees range, over extreme south-west Catalonia, and off the coast just east of Amposta. Surface O_3 concentrations range from 80 to 100 μg m^{-3} in these areas. Bias errors between the YSU scheme and the three other PBL schemes are similar with the Pyrenees and coastal maxima, with slightly better

Table 2
Statistics of surface meteorological variables; mean bias (*MB*) and linear correlation coefficient (*r*), between WRF model-simulations and METAR observations at Barcelona, Girona, and Reus. *MB* is calculated as WRF model – observed. Variables included in the analysis are 2-m air (T2) and dew point (TD2) temperature (in °C), and 10-m zonal (U10) and meridional (V10) wind components (in m s^{-1}).

PBL scheme								
	YSU		ACM2		MYNN2		BouLac	
	MB	*r*	*MB*	*r*	*MB*	*r*	*MB*	*r*
METAR - Barcelona								
T2	−1.86	0.93	−1.77	0.94	−1.85	0.94	−1.68	0.95
TD2	−1.44	0.71	−1.65	0.79	−1.39	0.78	−1.22	0.74
U10	−1.16	0.58	−1.07	0.57	−0.94	0.71	−0.87	0.63
V10	−0.79	0.96	−0.64	0.96	−0.72	0.97	−0.71	0.96
METAR – Girona								
T2	0.15	0.98	0.34	0.97	0.11	0.98	0.33	0.98
TD2	−1.59	0.29	−1.78	0.11	−1.69	0.35	−1.54	0.61
U10	0.43	0.10	0.65	0.13	0.63	0.23	0.77	0.35
V10	0.39	0.87	0.62	0.88	0.38	0.87	0.64	0.88
METAR – Reus								
T2	−2.56	0.97	−2.46	0.97	−2.63	0.98	−2.34	0.98
TD2	−1.38	0.65	−1.57	0.59	−1.26	0.67	−1.21	0.62
U10	−0.53	0.56	0.05	0.7	−0.17	0.75	−0.3	0.52
V10	−0.47	0.97	−0.22	0.98	−0.27	0.98	−0.56	0.98

performance by the MYNN2 and BouLac schemes with the maximum in far south-west Catalonia.

Next, we perform a similar analysis of spatial differences of surface NO_2 concentration (Fig. 8) between the various PBL schemes. In the morning, the maximum NO_2 concentrations (>60 μg m^{-3}) are focused along the coast from Reus to Girona, and inland west of Barcelona. CMAQ simulations with the ACM2 and MYNN2 schemes show mainly a negative bias, while the BouLac schemes shows a positive bias error.

By 12:00 UTC, the maximum NO_2 concentration has formed over the Barcelona metropolitan area, with values >60 μg m^{-3}. The mean bias for CMAQ simulations with all three PBL schemes is negative, with a slightly better performance by the BouLac scheme. In the evening, two main areas of maximum NO_2 concentrations have formed; one over extreme south-west Catalonia and another along the coast east of the pre-coastal mountain range. Under-estimates are shown with all three PBL schemes, with no clear favourite at this time of the day.

Finally, we examine the spatial differences of surface PM_{10} (Fig. 9) between the YSU (control run) and the three tested PBL schemes. A large area of surface PM_{10} (>15 μg m^{-3}) sits just offshore in the morning hours. CMAQ model-simulated PM_{10} with the MYNN2 scheme under-estimates the area by around 30%. The ACM2 and BouLac schemes mainly over-estimate the plume magnitude, with a slightly higher over-estimate from ACM2.

At 12:00 UTC the maximum area of PM_{10} is concentrated over the Sea between Amposta and Palma, with highest around 20 μg m^{-3} near Palma. All three CMAQ model simulations using different PBL schemes under-estimate the plume, however with a slightly lower bias error with the ACM2 scheme. In the evening, an area of high PM_{10} (>20 μg m^{-3}) forms along the coast just east of Girona. However, CMAQ simulations with all three PBL schemes strongly under-estimate (30–40%) the plume magnitude.

The differences between PBL schemes can be further highlighted by comparing daily grid-point values from the CMAQ model simulations to observations at six air quality stations for urban, suburban, and rural background station types. Mean bias (*MB*) and correlation (*r*) for each scheme is shown in Table 3. The statistics are calculated to represent the average performance of O_3, NO_2, and PM_{10} for each station type. Overall, the CMAQ model under-estimates all evaluated variables, no matter which PBL scheme is selected.

The CMAQ model performs the best with the comparisons of O_3 to observations. CMAQ model simulations with the ACM2 scheme have the lowest bias error with all station types, as low as −0.96 μg m^{-3} at urban sites. The correlation between CMAQ model and observations is the closest with rural stations (0.75–0.82), along with the second lowest *MB*.

Performance statistics show mixed results with surface NO_2 and PM_{10} concentrations against the observed values. At suburban and rural stations, CMAQ model simulations with the YSU and BouLac schemes perform well, with the YSU scheme slightly better ($MB = -6.48$ μg m^{-3} at suburban; $MB = -7.42$ μg m^{-3} at rural). Similar to surface O_3, the closest correlation of model to observations is associated with rural sites (0.53–0.57), however lower than O_3.

The performance of the CMAQ model in simulating PM_{10} was the worst of all variables analysed, both in terms of bias and correlation statistics. In addition, differences between CMAQ simulations with each PBL scheme are the closest of all variables. Low correlations between the CMAQ model and observations show a lack of confidence in the comparison. Similar to surface NO_2, CMAQ model simulations with the YSU and BouLac schemes show the best performance.

4. Summary and conclusions

This study evaluated the impact of four planetary boundary layer (PBL) parametrization schemes (two local, two non-local) from the Weather Research and Forecasting (WRF) mesoscale model on simulations of meteorological variables and predicted pollutant concentrations from the CALIOPE air quality forecast system (AQFS), maintained and operated at the Barcelona Supercomputing Center. The CALIOPE AQFS is composed of the WRF-ARW V3.5.1 meteorological model, HERMES v2 emissions model, CMAQ V5.0.2 chemical transport model, and dust outputs from BSC-DREAM8bv2.

The area of interest was the Catalonia region located in the northeast Iberian Peninsula during 7 May 2015, a day dominated by regional recirculations flow. Performance of the non-local schemes, Yonsei University (YSU; control run) and Assymetric Convective Model Version 2 (ACM2), and the local schemes, Mellor-Yamada-Janjic (MYJ) and Bougeault-Lacarrère (BouLac) were evaluated. AQFS-simulated pollutant concentrations were evaluated against six network urban, suburban, and rural background stations. In addition, we used METAR surface meteorological observations and vertical profiles from a radiosounding for an evaluation of the WRF simulations. Daytime WRF model-simulated PBL heights ere validated against estimates retrieved using a micro-pulse lidar system.

Large differences were found with the WRF model simulations of PBL height. WRF model simulations with all four PBL schemes under-estimated the height of the PBL when compared with estimates from

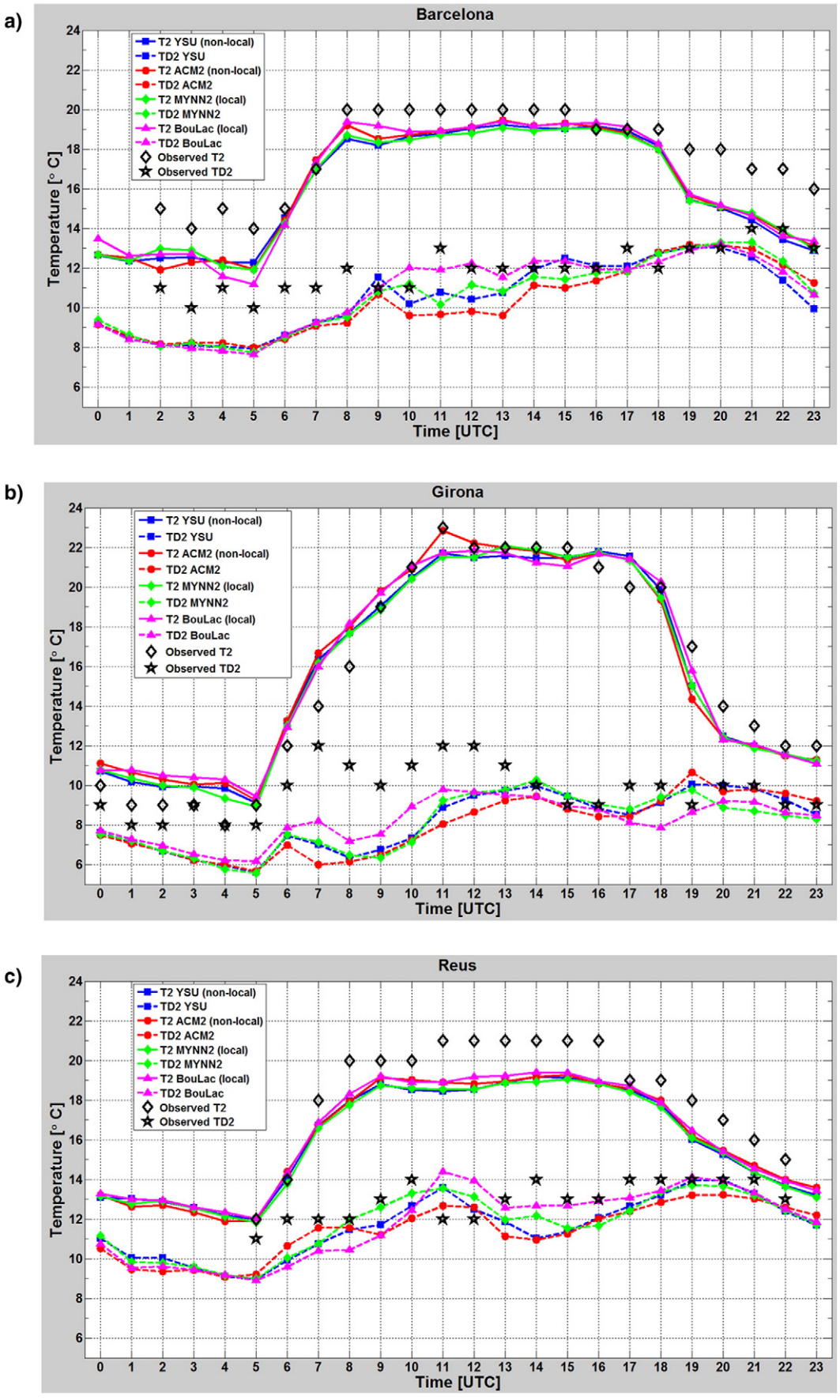

Fig. 4. Time series on 7 May 2015 of WRF model-simulated 2-m air temperature (T2; solid lines) and dew point temperature (TD2; dashed lines) against METAR observations at; a) Barcelona, b) Girona, and c) Reus.

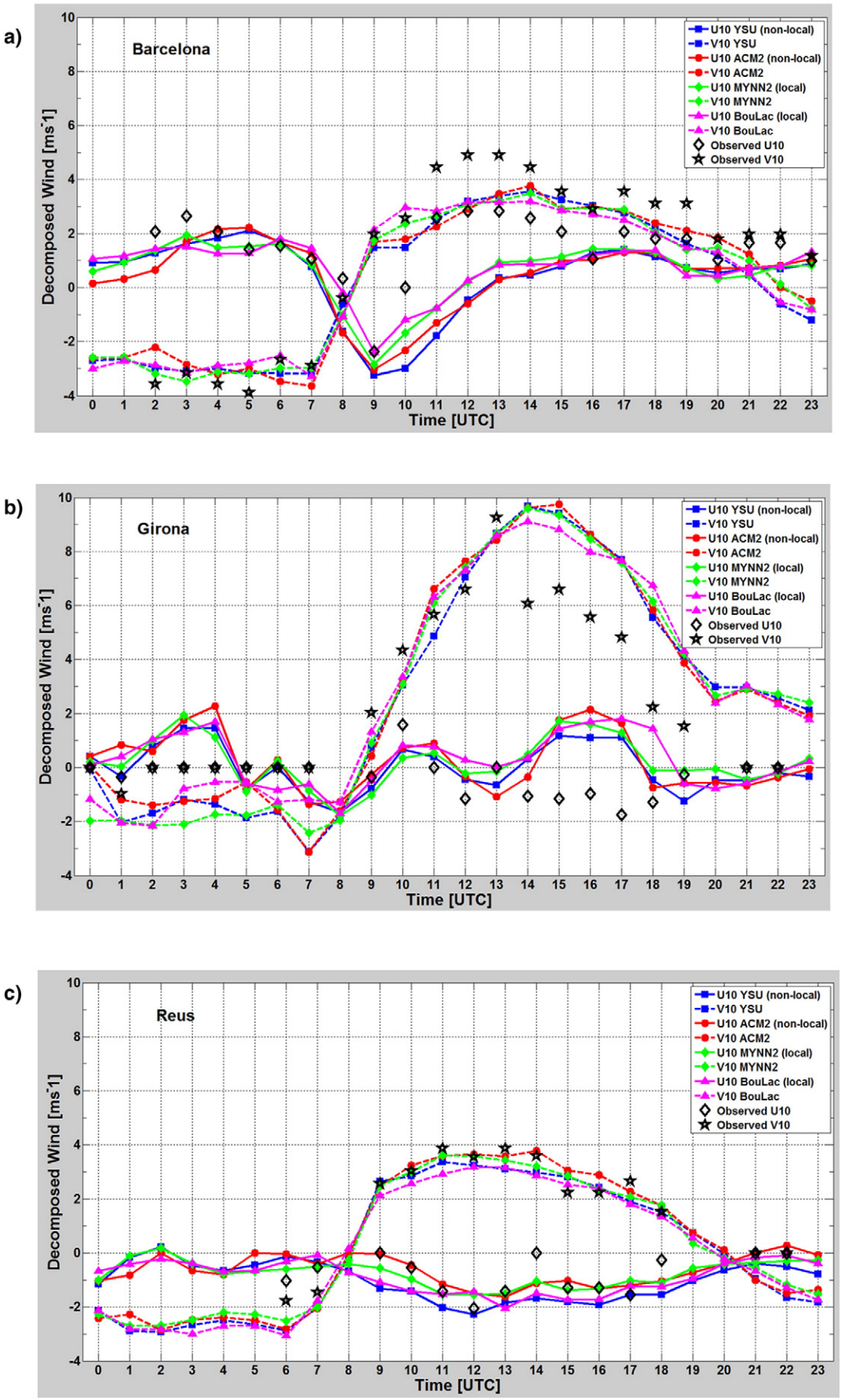

Fig. 5. Same as in Fig. 4, except for zonal (U10; solid lines) and meridional (V10; dashed lines) components of 10-m winds.

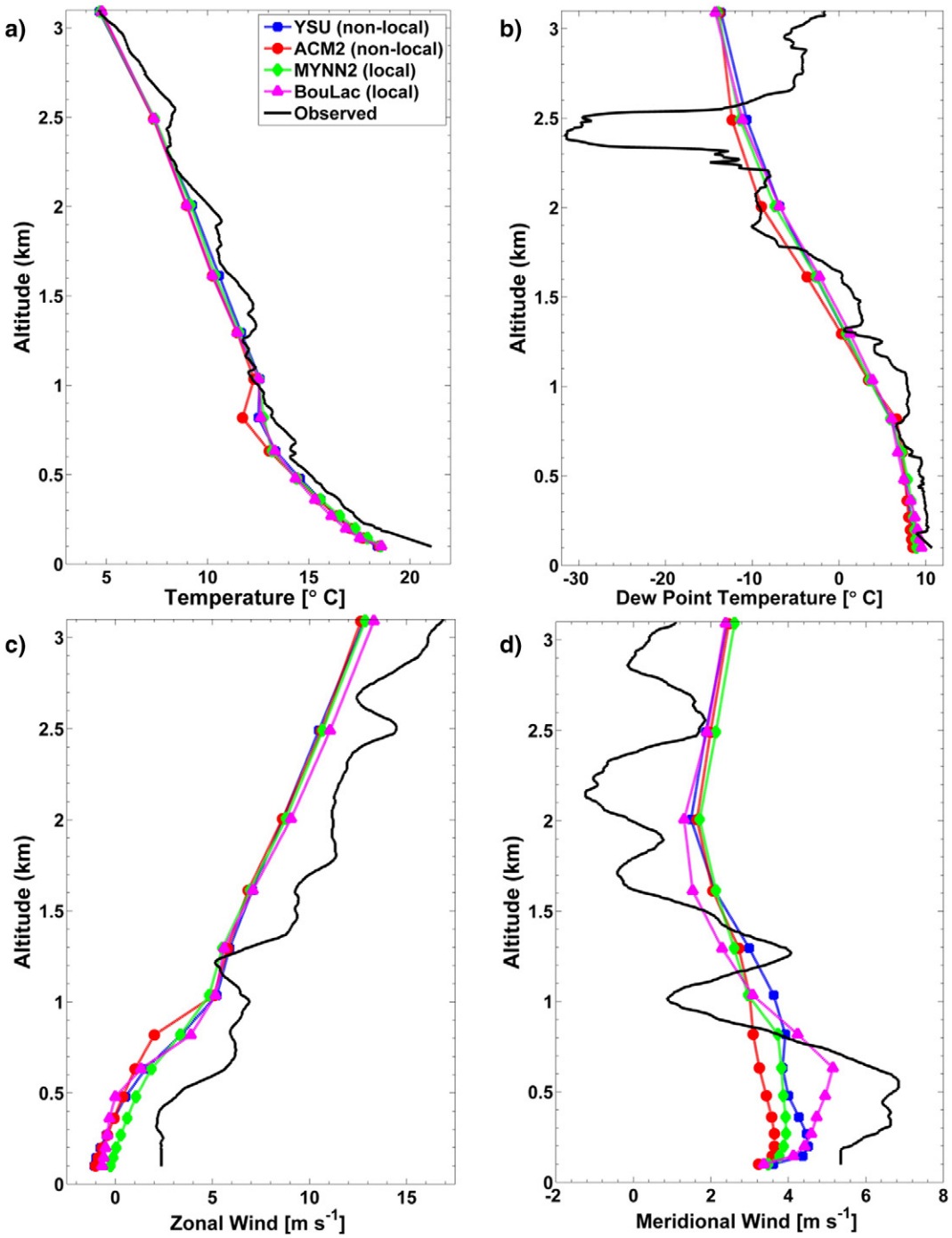

Fig. 6. Comparison of WRF model-simulated vertical profiles (colored lines and symbols) against a radiosounding (black solid line) on 7 May 2015 at 12:00 UTC for a) temperature, b) dew point temperature, c) zonal wind speed, and d) meridional wind speed.

the lidar. However, WRF model-simulated PBL height was best represented by a non-local scheme, such as ACM2 ($MB = 0.11$ km).

Surface meteorological variables showed ambiguous results, especially for 10 m zonal (U10) and meridional (V10) wind speed components, with under-estimates by the WRF model at Barcelona and Reus, and an over-estimate at Girona. The non-local YSU and ACM2 schemes simulated the closest values to the observations. 2-m air temperature (T2) and dew point temperature (TD2) were most accurately represented by a local PBL scheme, with the best performance from the BouLac scheme.

The comparison of WRF model vertical profiles against a 12:00 UTC radiosounding showed the largest biases with zonal and meridional winds. Overall, non-local schemes provided the lowest biases in the boundary layer. Local PBL schemes, such as BouLac, showed the closest temperature and dew point temperature to the observed values. However, no PBL scheme could help to resolve an extreme dry layer in the lower atmosphere.

The best performances from the CMAQ simulations were with the surface ozone (O_3) and nitrogen dioxide (NO_2) concentrations. Local PBL schemes, BouLac and MYNN2, showed the lowest bias error against the control run when comparing spatially. Performance statistics of the CMAQ model against observations showed the BouLac scheme with a low mean bias for NO_2, while the non-local ACM2 performed well with O_3.

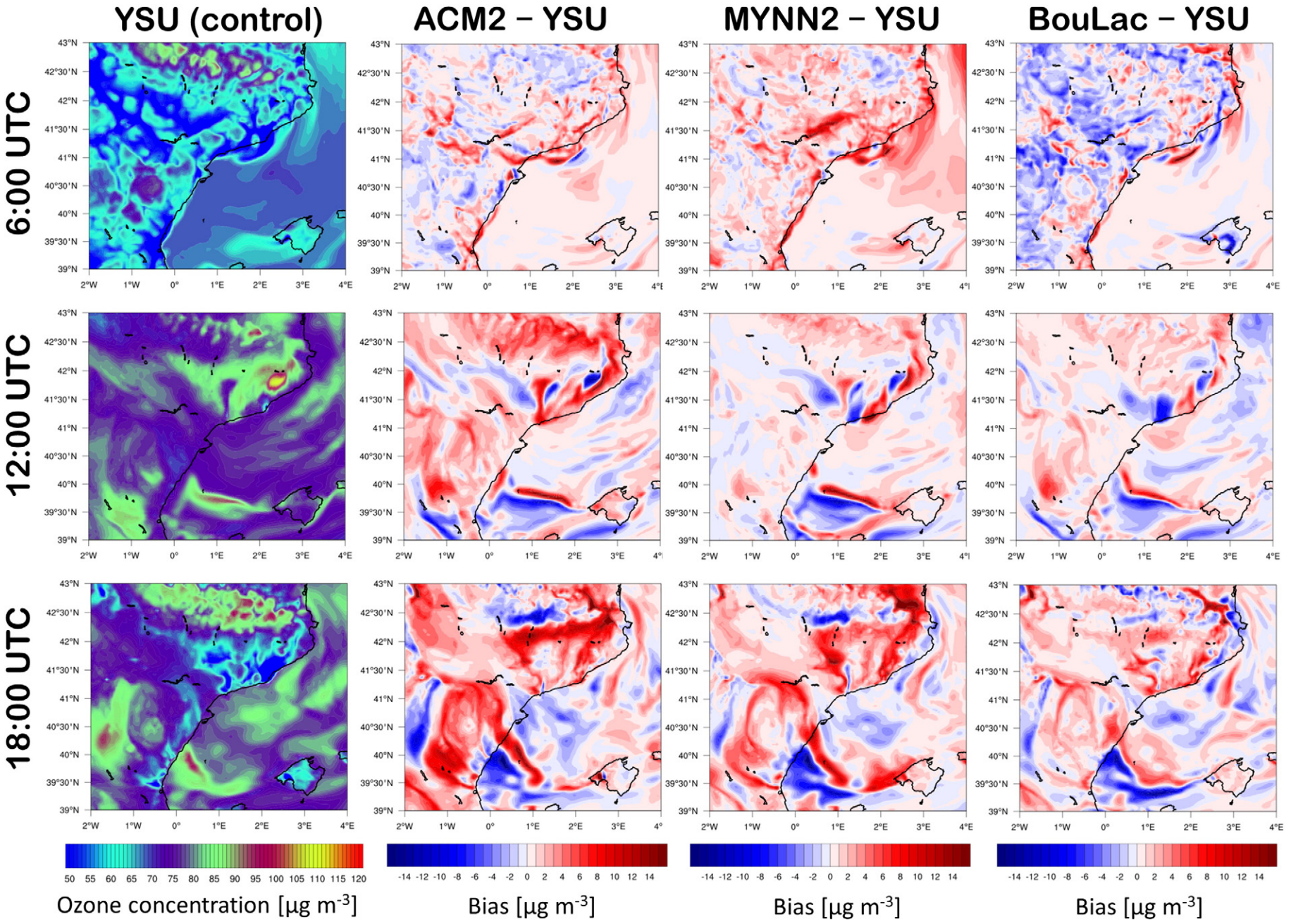

Fig. 7. Spatial comparison of CALIOPE-simulated surface ozone concentration (O_3) from the control run (YSU; first column), and bias between tested WRF PBL schemes and the control run for the ACM2 (column 2), MYNN2 (column 3), and BouLac (column 4) schemes. Plots are shown for 6:00 UTC (first row), 12:00 UTC (second row), and 18:00 UTC (third row) on 7 May 2015.

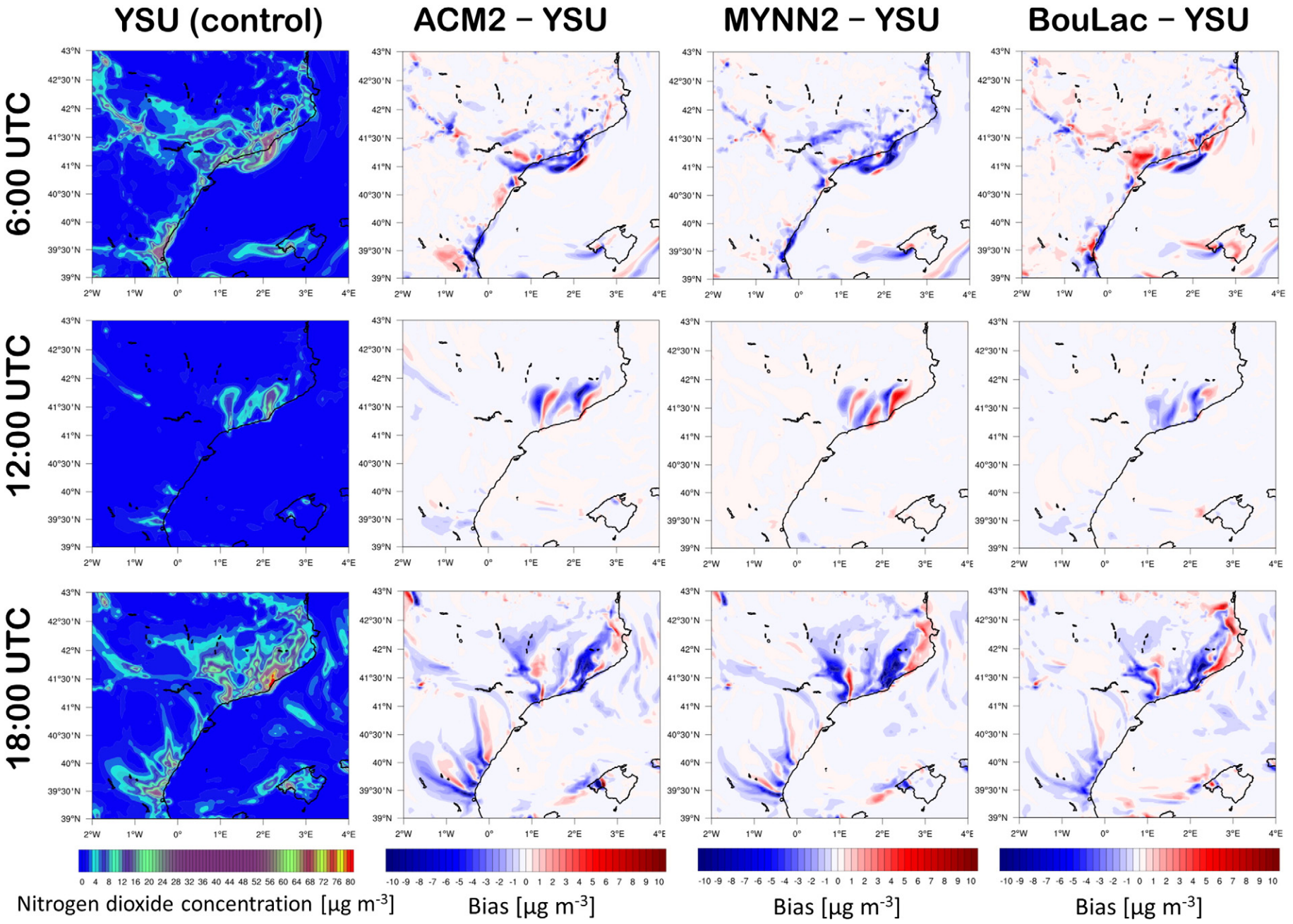

Fig. 8. Same as in Fig. 7, except for surface concentration of nitrogen dioxide (NO_2).

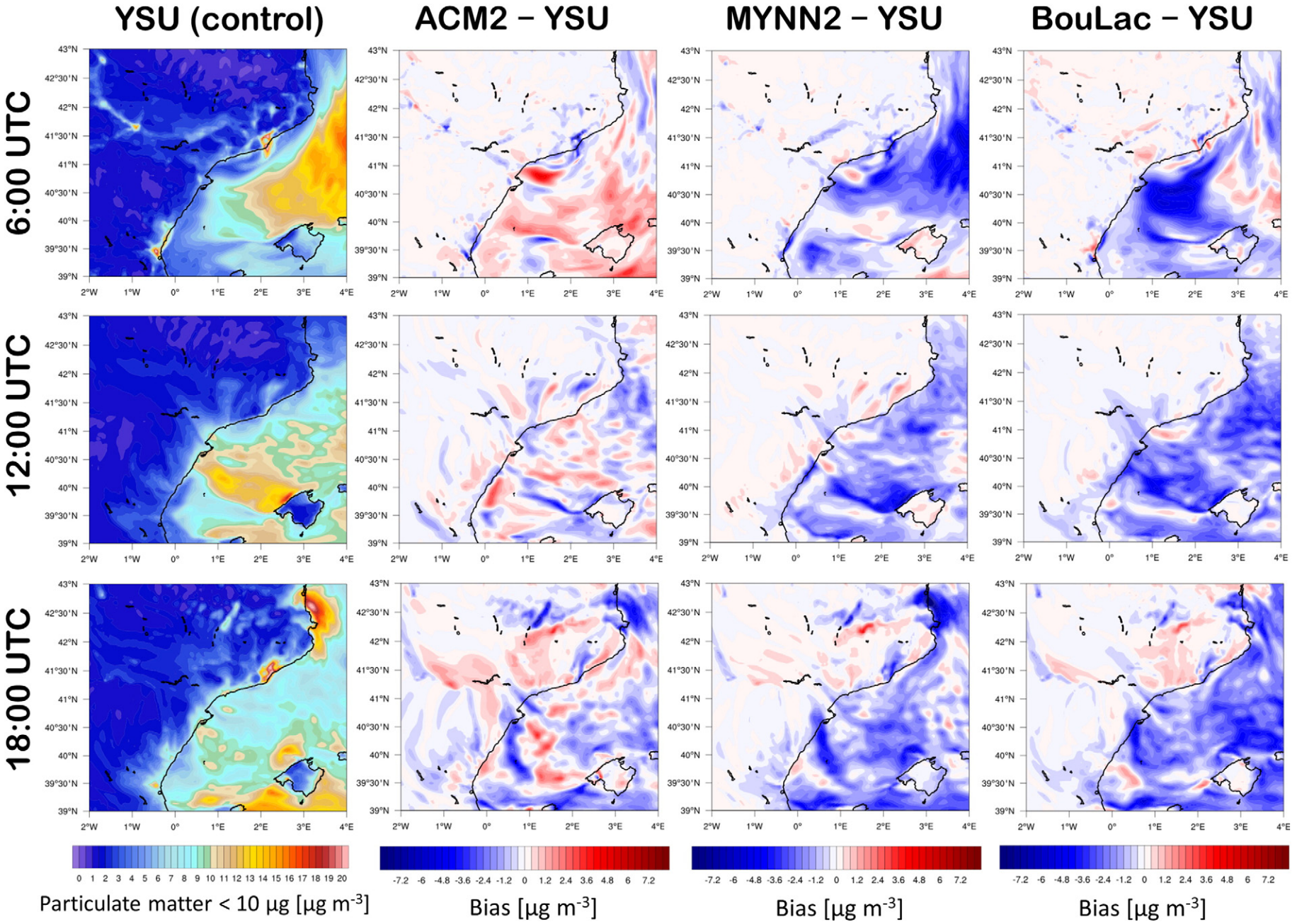

Fig. 9. Same as in Fig. 7, except for surface concentration of particulate matter <10 μm (PM_{10}).

Table 3
Statistics of surface photochemical and aerosol variables; mean bias (*MB*) and linear correlation coefficient (*r*), between CALIOPE AQFS-simulations and network observations at urban, suburban, and rural background stations. Two stations are averaged for each station type (shown in Fig. 1d). *MB* is calculated as CALIOPE AQFS – observed. Variables included (in units $\mu g\ m^{-3}$) are surface ozone (O_3), nitrogen dioxide (NO_2), and particulate matter <10 μm (PM_{10}).

PBL scheme								
	YSU		ACM2		MYNN2		BouLac	
	MB	*r*	*MB*	*r*	*MB*	*r*	*MB*	*r*
Urban								
O_3	−2.53	0.53	−0.96	0.54	−1.6	0.51	−2.01	0.55
NO_2	−17.44	0.22	−18.1	0.2	−17.58	0.22	−17.14	0.24
PM_{10}	−28.63	0.15	−28.68	0.28	−28.76	0.22	−28.77	0.22
Suburban								
O_3	−14.69	0.72	−12.75	0.56	−12.78	0.58	−13.04	0.74
NO_2	−6.48	0.57	−7.36	0.44	−6.99	0.47	−7.27	0.56
PM_{10}	−16.29	0.2	−16.61	0.13	−16.81	0.11	−17.05	0.2
Rural								
O_3	−8.23	0.75	−6.27	0.82	−7.94	0.81	−8.34	0.79
NO_2	−7.42	0.57	−7.57	0.57	−7.54	0.54	−7.48	0.53
PM_{10}	−12.84	0.05	−12.77	0.39	−12.75	0.39	−12.72	0.37

Surface particulate matter <10 μm (PM_{10}) showed the worst performance of all the air quality variables evaluated, with low correlations between the CMAQ model and observations. The poor performance of CMAQ model-simulated PM_{10} is possibly attributed to poor simulations of the PBL height from the WRF model. However, other sources of the uncertainty could include emissions from the HERMES model and conversion factors from CMAQ.

In conclusion, we found that a non-local PBL scheme (ACM2) performs well for model simulations of the PBL height and surface and upper-air winds. In contrast, a local scheme (BouLac) is preferred for surface air and dew point temperature. In addition, the ACM2 and BouLac schemes performed better than the YSU (control run) scheme for air quality simulations. Further studies are needed to determine if the current PBL scheme in the CALIOPE AQFS should be changed.

Acknowledgements

The research leading to these results has received funding from the European Union Seventh Framework Programme (FP7/2007-2013): People, ITN Marie Curie Actions Programme (2012–2016) in the frame of ITaRS under grant agreement no. 289923. Simulations were executed on the MareNostrum supercomputer at the Barcelona Supercomputing Centre, under grants SEV-2011-00067 of Severo Ochoa program and CGL2013-46736-R, awarded by the Spanish Government. Special thanks to Francesc Rocadenbosch and the UPC Remote Sensing Laboratory for use of the extended Kalman filter technique. The authors wish to thank Victor Valverde for his assistance with the air quality simulations.

References

Baldasano, J.M., Cremades, L., Soriano, C., 1994. Circulation of air pollutants over the Barcelona geographical area in summer. Proceedings of Sixth European Symposium Physico-Chemical Behavior of Atmospheric Pollutants, pp. 474–479 (Report EUR 15609/1 EN, Varese).

Baldasano, J.M., Jiménez-Guerrero, P., Jorba, O., Pérez, C., López, E., Güereca, P., Martín, F., Vivanco, M.G., Palomino, I., Querol, X., Pandolfi, M., Sanz, M.J., Diéguez, J.J., 2008. Caliope: an operational air quality forecasting system for the Iberian peninsula, Balearic Islands and Canary Islands – first annual evaluation and ongoing developments. Adv. Sci. Res. 2 (1), 89–98. http://dx.doi.org/10.5194/asr-2-89-2008.

Baldasano, J.M., Pay, M.T., Jorba, O., Gassó, S., Jiménez-Guerrero, P., 2011. An annual assessment of air quality with the CALIOPE modeling system over Spain. Sci. Total Environ. 409 (11), 2163–2178. http://dx.doi.org/10.1016/j.scitotenv.2011.01.041.

Banks, R.F., Tiana-Alsina, J., María Baldasano, J., Rocadenbosch, F., 2014. Retrieval of boundary layer height from lidar using extended Kalman filter approach, classic methods, and backtrajectory cluster analysis. Proc. SPIE 9242, 92420F. http://dx.doi.org/10.1117/12.2072049.

Banks, R.F., Tiana-Alsina, J., Rocadenbosch, F., Baldasano, J.M., 2015. Performance evaluation of the boundary-layer height from lidar and the weather research and forecasting model at an urban coastal site in the North-East Iberian Peninsula. Bound.-Layer Meteorol. http://dx.doi.org/10.1007/s10546-015-0056-2.

Banks, R.F., Tiana-Alsina, J., Baldasano, J.M., Rocadenbosch, F., Papayannis, A., Solomos, S., Tzanis, C.G., 2016. Sensitivity of boundary layer variables to PBL schemes in the WRF model based on surface meteorological observations, lidar, and radiosondes during the HygrA-CD campaign. Atmos. Res. http://dx.doi.org/10.1016/j.atmosres.2016.02.024.

Basart, S., Pay, M.T., Jorba, O., Perez, C., Jimenez-Guerrero, P., Schulz, M., Baldasano, J.M., 2012. Aerosols in the CALIOPE air quality modelling system: evaluation and analysis of PM levels, optical depths and chemical composition over Europe. Atmos. Chem. Phys. 12 (7), 3363–3392. http://dx.doi.org/10.5194/acp-12-3363-2012.

Blackadar, A.K., 1978. Modeling pollutant transfer during daytime convection. Preprints Fourth Symposium on Atmospheric Turbulence, Diffusion, and Air Quality. American Meteorological Society, Reno, pp. 443–447.

Bossioli, E., Tombrou, M., Dandou, A., Athanasopoulou, E., Varotsos, K.V., 2009. The role of planetary boundary-layer parameterizations in the air quality of an urban area with complex topography. Bound.-Layer Meteorol. 131 (1), 53–72. http://dx.doi.org/10.1007/s10546-009-9349-7.

Bougeault, P., Lacarrere, P., 1989. Parameterization of orography-induced turbulence in a Mesobeta–scale model. Mon. Weather Rev. 117 (8), 1872–1890. http://dx.doi.org/10.1175/1520-0493(1989)117<1872:POOITI>2.0.CO;2.

Cheng, F.Y., Chin, S.C., Liu, T.H., 2012. The role of boundary layer schemes in meteorological and air quality simulations of the Taiwan area. Atmos. Environ. 54, 714–727. http://dx.doi.org/10.1016/j.atmosenv.2012.01.029.

Cuchiara, G.C., Li, X., Carvalho, J., Rappenglück, B., 2014. Intercomparison of planetary boundary layer parameterization and its impacts on surface ozone concentration in the WRF/Chem model for a case study in Houston/Texas. Atmos. Environ 96, 175–185. http://dx.doi.org/10.1016/j.atmosenv.2014.07.013.

Draxler, R.R., Rolph, G.D., 2013. HYSPLIT (HYbrid Single-Particle Lagrangian Integrated Trajectory). (NOAA Air Resour. Lab. Coll. Park. MD [online] Available from: http://www.arl.noaa.gov/HYSPLIT.php).

Dudhia, J., 1989. Numerical study of convection observed during the winter monsoon experiment using a mesoscale two-dimensional model. J. Atmos. Sci 46 (20), 3077–3107. http://dx.doi.org/10.1175/1520-0469(1989)046<3077:NSOCOD>2.0.CO;2.

Dudhia, J., 1993. A non-hydrostatic version of the Penn State-NCAR mesoscale model: validation tests and simulation of an Atlantic cyclone and cold front. Mon. Weather Rev. 121, 1493–1513.

Folberth, G.A., Hauglustaine, D.A., Lathière, J., Brocheton, F., 2006. Interactive chemistry in the Laboratoire de Météorologie Dynamique general circulation model: model description and impact analysis of biogenic hydrocarbons on tropospheric chemistry. Atmos. Chem. Phys 6 (8), 2273–2319. http://dx.doi.org/10.5194/acp-6-2273-2006.

Gan, C.M., Wu, Y., Madhavan, B.L., Gross, B., Moshary, F., 2011. Application of active optical sensors to probe the vertical structure of the urban boundary layer and assess anomalies in air quality model PM2.5 forecasts. Atmos. Environ. 45 (37), 6613–6621. http://dx.doi.org/10.1016/j.atmosenv.2011.09.013.

Goncalves, M., Jimenez-Guerrero, P., Baldasano, J.M., 2009. Contribution of atmospheric processes affecting the dynamics of air pollution in South-Western Europe during a typical summertime photochemical episode. Atmos. Chem. Phys. 849–864. http://dx.doi.org/10.5194/acpd-8-18457-2008.

Gangoiti, G., Millán, M.M., Salvador, R., Mantilla, E., 2001. Long-range transport and recirculation of pollutants in the western Mediterranean during the project regional cycles of air pollution in the west-central Mediterranean area. Atmos. Environ. 35, 6267–6276.

Guerreiro, C., de Leeuw, F., Foltescu, V., Schilling, J., van Aardenne, J., Lükewille, A., Adams, M., 2012. Air Quality in Europe - 2012 Report, EEA Report No 4/2012.

Hauglustaine, D.A., Hourdin, F., Jourdain, L., Filiberti, M.-A., Walters, S., Lamarque, J.-F., Holland, E.A., 2004. Interactive chemistry in the Laboratoire de Météorologie Dynamique general circulation model: description and background tropospheric chemistry evaluation. J. Geophys. Res. Atmos 109 (D4), D04314. http://dx.doi.org/10.1029/2003JD003957.

Hong, S.Y., 2010. A new stable boundary-layer mixing scheme and its impact on the simulated East Asian summer monsoon. Q. J. R. Meteorol. Soc. 136 (651), 1481–1496. http://dx.doi.org/10.1002/qj.665.

Hong, S.-Y., Pan, H.-L., 1996. Nonlocal boundary layer vertical diffusion in a medium-range forecast model. Mon. Weather Rev. 124 (10), 2322–2339. http://dx.doi.org/10.1175/1520-0493(1996)124<2322:NBLVDI>2.0.CO;2.

Hong, S.-Y., Dudhia, J., Chen, S.-H., 2004. A revised approach to ice microphysical processes for the bulk parameterization of clouds and precipitation. Mon. Weather Rev. 132 (1), 103–120. http://dx.doi.org/10.1175/1520-0493(2004)132<0103:ARATIM>2.0.CO;2.

Hong, S.-Y., Noh, Y., Dudhia, J., 2006. A new vertical diffusion package with an explicit treatment of entrainment processes. Mon. Weather Rev. 134 (9), 2318–2341. http://dx.doi.org/10.1175/MWR3199.1.

Kain, J.S., 2004. The Kain–Fritsch convective parameterization: an update. J. Appl. Meteorol 43 (1), 170–181. http://dx.doi.org/10.1175/1520-0450(2004)043<0170:TKCPAU>2.0.CO;2.

Kim, Y., Fu, J.S., Miller, T.L., 2010. Improving ozone modeling in complex terrain at a fine grid resolution: part I - examination of analysis nudging and all PBL schemes associated with LSMs in meteorological model. Atmos. Environ. 44 (4), 523–532. http://dx.doi.org/10.1016/j.atmosenv.2009.10.045.

Jorba, O., Pérez, C., Rocadenbosch, F., Baldasano, J.M., 2004. Cluster analysis of 4-day back trajectories arriving in the Barcelona area (Spain) from 1997 to 2002. J. Appl. Meteorol 43 (6), 887–901.

Lange, D., Tiana-Alsina, J., Saeed, U., Tomás, S., Rocadenbosch, F., 2014. Atmospheric boundary layer height monitoring using a kalman filter and backscatter lidar returns. IEEE Trans. Geosci. Remote Sens. 52 (8), 4717–4728. http://dx.doi.org/10.1109/TGRS.2013.2284110.

Lange, D., Rocadenbosch, F., Tiana-alsina, J., Frasier, S., Member, S., 2015. Atmospheric-boundary-layer height estimation using a Kalman filter and a frequency-modulated continuous-wave radar. IEEE Trans. Geosci. Remote Sens. 53 (6), 3338–3349. http://dx.doi.org/10.1109/TGRS.2014.2374233.

Mao, Q., Gautney, L.L., Cook, T.M., Jacobs, M.E., Smith, S.N., Kelsoe, J.J., 2006. Numerical experiments on MM5-CMAQ sensitivity to various PBL schemes. Atmos. Environ. 40 (17), 3092–3110. http://dx.doi.org/10.1016/j.atmosenv.2005.12.055.

Martilli, A., Clappier, A., Rotach, M.W., 2002. An urban surface exchange parameterisation for mesoscale models. Boundary-Layer Meteorol. 104 (2), 261–304. http://dx.doi.org/10.1023/A:1016099921195.

Misenis, C., Zhang, Y., 2010. An examination of sensitivity of WRF/Chem predictions to physical parameterizations, horizontal grid spacing, and nesting options. Atmos. Res. 97 (3), 315–334. http://dx.doi.org/10.1016/j.atmosres.2010.04.005.

Mlawer, E.J., Taubman, S.J., Brown, P.D., Iacono, M.J., Clough, S.A., 1997. Radiative transfer for inhomogeneous atmospheres: RRTM, a validated correlated-k model for the longwave. J. Geophys. Res. 102 (D14), 16663. http://dx.doi.org/10.1029/97JD00237.

Nakanishi, M., Niino, H., 2006. An improved Mellor-Yamada level-3 model: its numerical stability and application to a regional prediction of advection fog. Boundary-Layer Meteorol. 119 (2), 397–407. http://dx.doi.org/10.1007/s10546-005-9030-8.

Pay, M.T., Piot, M., Jorba, O., Gassó, S., Gonçalves, M., Basart, S., Dabdub, D., Jiménez-Guerrero, P., Baldasano, J.M., 2010. A full year evaluation of the CALIOPE-EU air quality modeling system over Europe for 2004. Atmos. Environ 44 (27), 3322–3342. http://dx.doi.org/10.1016/j.atmosenv.2010.05.040.

Pay, M.T., Jiménez-Guerrero, P., Baldasano, J.M., 2011. Implementation of resuspension from paved roads for the improvement of CALIOPE air quality system in Spain. Atmos. Environ. 45, 802–807. http://dx.doi.org/10.1016/j.atmosenv.2010.10.032.

Pay, M.T., Jiménez-Guerrero, P., Baldasano, J.M., 2012a. Assessing sensitivity regimes of secondary inorganic aerosol formation in Europe with the CALIOPE-EU modeling system. Atmos. Environ. 51, 146–164. http://dx.doi.org/10.1016/j.atmosenv.2012.01.027.

Pay, M.T., Jiménez-Guerrero, P., Jorba, O., Basart, S., Querol, X., Pandolfi, M., Baldasano, J.M., 2012b. Spatio-temporal variability of concentrations and speciation of particulate matter across Spain in the CALIOPE modeling system. Atmos. Environ. 46, 376–396. http://dx.doi.org/10.1016/j.atmosenv.2011.09.049.

Pay, M.T., Martínez, F., Guevara, M., Baldasano, J.M., 2014. Air quality forecasts at kilometer scale grid over Spanish complex terrains. Geosci. Model Dev. Discuss. 7 (2), 2293–2334. http://dx.doi.org/10.5194/gmdd-7-2293-2014.

Pérez, C., Jiménez, P., Jorba, O., Sicard, M., Baldasano, J.M., 2006. Influence of the PBL scheme on high-resolution photochemical simulations in an urban coastal area over the western Mediterranean. Atmos. Environ 40 (27), 5274–5297. http://dx.doi.org/10.1016/j.atmosenv.2006.04.039.

Pleim, J.E., 2007. A combined local and nonlocal closure model for the atmospheric boundary layer. Part I: model description and testing. J. Appl. Meteorol. Climatol. 46 (9), 1383–1395. http://dx.doi.org/10.1175/JAM2539.1.

Rocadenbosch, F., Vázquez, G., Comerón, A., 1998. Adaptive filter solution for processing lidar returns: optical parameter estimation. Appl. Opt. 37 (30), 7019–7034. http://dx.doi.org/10.1364/AO.37.007019.

Rocadenbosch, F., Soriano, C., Comerón, A., Baldasano, J.M., 1999. Lidar inversion of atmospheric backscatter and extinction-to-backscatter ratios by use of a Kalman filter. Appl. Opt. 38 (15), 3175–3189.

Roeckner, E., Brokopf, R., Esch, M., Giorgetta, M.a., Hagemann, S., Kornblueh, L., Manzini, E., Schlese, U., Schulzweida, U., 2006. Sensitivity of simulated climate to horizontal and vertical resolution in the ECHAM5 atmosphere model. J. Clim. 19 (16), 3771–3791. http://dx.doi.org/10.1175/JCLI3824.1.

Rouil, L., Honoré, C., Vautard, R., Beekman, M., Bessagnet, B., Malherbe, L., Meleux, F., Dufour, A., Elichegaray, C., Flaud, J.M., Menut, L., Martin, D., Peuch, A., Peuch, V.H., Poisson, N., 2009. Prev'air: an operational forecasting and mapping system for air quality in Europe. Bull. Am. Meteorol. Soc. 90 (1), 73–83. http://dx.doi.org/10.1175/2008BAMS2390.1.

Schaap, M., Hendriks, C., Kranenburg, R., 2015. Performance of European chemistry transport models as function of horizontal resolution. Unece. Org 112, 90–105. http://dx.doi.org/10.1016/j.atmosenv.2015.04.003.

Sicardi, V., Ortiz, J., Rincón, A., Jorba, O., Pay, M.T., Gassó, S., Baldasano, J.M., 2012. Assessment of Kalman filter bias-adjustment technique to improve the simulation of ground-level ozone over Spain. Sci. Total Environ. 416, 329–342. http://dx.doi.org/10.1016/j.scitotenv.2011.11.050.

Skamarock, W.C., Klemp, J.B., 2008. A time-split nonhydrostatic atmospheric model for weather research and forecasting applications. J. Comput. Phys. 227 (7), 3465–3485. http://dx.doi.org/10.1016/j.jcp.2007.01.037.

Skamarock, W.C., Klemp, J.B., Dudhia, J., Gill, D.O., Barker, D.M., Wang, W., Powers, J.G., 2005. A Description of the Advanced Research WRF Version 2.

Soret, A., Jimenez-Guerrero, P., Baldasano, J.M., 2011. Comprehensive air quality planning for the Barcelona metropolitan area through traffic management. Atmos. Pollut. Res. 2 (2011), 255–266. http://dx.doi.org/10.5094/APR.2011.032.

Spinhirne, J.D., Rall, J.A.R., Scott, V.S., 1995. Compact eye safe lidar systems. Rev. Laser Eng. 23, 112–118.

Tewari, M., et al., 2004. Implementation and verification of the unified NOAH land surface model in the WRF model. 20th Conference on Weather Analysis and Forecasting/16th Conference on Numerical Weather Prediction, pp. 11–15.

Welton, E., Campbell, J., Spinhirne, J., Scott, V., 2001. Global monitoring of clouds and aerosols using a network of micro-pulse lidar systems,. Proc. SPIE 4153, 151–158.

Zhang, K., Wan, H., Wang, B., Zhang, M., Feichter, J., Liu, X., 2010. Tropospheric aerosol size distributions simulated by three online global aerosol models using the M7 microphysics module. Atmos. Chem. Phys. Discuss. 10 (3), 5803–5861. http://dx.doi.org/10.5194/acpd-10-5803-2010.

Zhang, Y., Bocquet, M., Mallet, V., Seigneur, C., Baklanov, A., 2012. Real-time air quality forecasting, part I: history, techniques, and current status. Atmos. Environ. 60, 632–655. http://dx.doi.org/10.1016/j.atmosenv.2012.06.031.